Computers in Biology and Medicine 115 (2019) 103446

Contents lists available at ScienceDirect

Computers in Biology and Medicine

journal homepage: http://www.elsevier.com/locate/compbiomed

Automated detection of shockable and non-shockable arrhythmia using novel wavelet-based ECG features

Manish Sharma [a,*], Swapnil Singh [b], Abhishek Kumar [c], Ru San Tan [d], U. Rajendra Acharya [e,f,g]

[a] Department of Electrical Engineering, Institute of Infrastructure Technology Research and Management, Ahmedabad, India
[b] Department of Project Management, National Institute of Industrial Engineering, Mumbai, India
[c] Department of Civil Engineering, Indian Institute of Technology, Madras, India
[d] Department of Cardiology, National Heart Care Centre Singapore, Singapore
[e] Department of Electronics and Computer Engineering, Ngee Ann Polytechnic, Singapore, 599489, Singapore
[f] Department of Biomedical Engineering, School of Science and Technology, SUSS, Singapore
[g] International Research Organization for Advanced Science and Technology (IROAST) Kumamoto University, Kumamoto, Japan

ARTICLE INFO

Keywords:
Shockable
Heart
ECG
Wavelets
Optimization problem
Machine learning
Semi-definite program
Filter design
Classification

ABSTRACT

Malignant arrhythmia can lead to sudden cardiac death (SCD). Shockable arrhythmia can be terminated with device electrical shock therapies. Ventricular-tachycardia (VT) and ventricular fibrillation (VF) are responsive to electrical anti-tachycardia pacing therapy and defibrillation which help to restore normal electrical and mechanical function of the heart. In contrast, non-shockable arrhythmia like asystole and bradycardia are not responsive to electric shock therapy. Distinguishing between shockable and non-shockable arrhythmia is an important diagnostic challenge that has practical clinical relevance. It is difficult to accurately differentiate between these two types of arrhythmia by manual inspection of electrocardiogram (ECG) segments within the short time duration before triggering the device for electrical therapy. Automated defibrillators are equipped with automatic shockable arrhythmia detection algorithms based on ECG morphological features, which may possess variable diagnostic performance depending on machine models. In our work, we have designed a robust system using wavelet decomposition filter banks for extraction of features from the ECG signal and then classifying the features. We believe this method will improve the accuracy of discriminating between shockable and non-shockable arrhythmia compared with existing conventional algorithms. We used a novel three channel orthogonal wavelet filter bank, which extracted features from ECG epochs of duration 2 s to distinguish between shockable and non-shockable arrhythmia. The fuzzy, Renyi and sample entropies are extracted from the various wavelet coefficients and fed to support vector machine (SVM) classifier for automated classification. We have obtained an accuracy of 98.9%, sensitivity and specificity of 99.08% and 97.11.9%, respectively, using 10-fold cross validation. The area under the receiver operating characteristic has been found to be 0.99 with F1-score of 0.994. The system developed is more accurate than the existing algorithms. Hence, the proposed system can be employed in automated defibrillators inside and outside hospitals for emergency revival of patients suffering from SCD. These automated defibrillators can also be implanted inside the human body for automatic detection of potentially fatal shockable arrhythmia and to deliver an appropriate electric shock to the heart.

1. Introduction

Cardiac arrest or sudden cardiac death (SCD) is the condition in which the heart stops pumping [1,2]. Unless the victim is resuscitated promptly, this can cause either death or catastrophic neurological deficits. SCD can happen due to heart attack or disease of the electrical conduction system of the heart, which can be from acquired or genetic conditions. Usually there is a narrow time window for resuscitative treatment during SCD. More than a million people die every year in United States alone due to SCD.

Approximately 10.3% of the total deaths occurring in India are due to SCD. Electrocardiogram (ECG) diagnosis [3] is very important to decide whether the cardiac arrest is due to non-shockable (Fig. 1) or shockable arrhythmia (Fig. 2). Shockable arrhythmia includes

* Corresponding author.
E-mail addresses: manishsharma.iitb@gmail.com (M. Sharma), tan.ru.san@singhealth.com.sg (R. San Tan), aru@np.edu.sg (U.R. Acharya).

https://doi.org/10.1016/j.compbiomed.2019.103446
Received 30 July 2019; Received in revised form 13 September 2019; Accepted 13 September 2019
Available online 18 September 2019

ventricular fibrillation (VF) [4] and ventricular tachycardia (VT) [5–7]. In the case of VF (Table 1), the ECG shows irregular and rapid QRS complexes. In the case of VT, the ECG is rapid and regular with broad QRS complexes [8]. Non-shockable arrhythmias include asystole and bradycardia. In asystole, no electrical activity is observed in the heart and hence the ECG shows a flatline. Once it is decided whether the arrhythmia is of shockable or non-shockable type, the patient is treated accordingly. If it is a shockable one, then it is amenable to electric shock therapy or defibrillation. These defibrillators are of vital importance in the medical field because of their fast and accurate response. The American Health Association (AHA) recommends treatment with defibrillators within 3 min for in-hospital cardiac arrest and in under 5 min for out-of-hospital events [9–12]. In the case of non-shockable cardiac arrests, defibrillation is not helpful and cardio-pulmonary resuscitation (CPR) should continue to be performed to sustain the cardiac output [13–15].

For proper automated diagnosis of shockable rtythm (SAR) and non-shockable rhythm (NSAR) using ECG signals, it is highly desirable to have automated algorithms which are highly refined, optimized, and accurate in discriminating between the two types of arrhythmia. In the subsequent text, we discuss a few best existing automated algorithms developed to distinguish between shockable and non-shockable fatal arrhythmia [16].

In 2007, Amann et al. [17] developed a methodology using twelve different time delay methods and obtained an accuracy of 96.2%. In the same year, Fokkenrood et al. [18] employed an amplitude distribution analysis method for discrimination of shockable and non-shockable rhythms and obtained accuracy of 98%. In 2014, Li et al. [19] used a ventricular fibrillation filter leakage method and obtained an accuracy of 96.3%. Tripathy et al. [20] employed the methodology of variational mode decomposition (VMD) and Renyi entropy (RE) features and obtained an accuracy of 97.23%. Recently, Acharaya et al. [21] implemented a convolutional neural network (CNN) methodology and reported an accuracy of 93.18%.

In this work, we have proposed optimal wavelet-based automated system to identify shockable arrhythmia. The entropy features are extracted from the SBs of the optimal three channel wavelet filter banks [22–26]. The objective of our study is to design a fast, accurate, robust and reliable wavelet-based automated system that can discriminate between shockable and non-shockable arrhythmia for automated defibrillators [27–30].

2. Dataset used

The data utilized in this work was obtained from three sources namely, the MIT-BIH database for arrhythmia (MITDBA), MIT-BIH database for fatal ventricular arrhythmia (FVADB) and database for ventricular tachyarrhythmia from Creighton University (VTADB) [31]. We sampled the data obtained from MITDBA consisting of forty-eight dual channel ECG samples of length 30 min at a rate of 250 Hz. The data of FVADB consisted of 22 two lead ECG samples of length 35 min and were sampled at a rate of 250 Hz. The data from VTADB consisted of 35 mono channel ECG signals of length 8 min and were also sampled at 250 Hz. All the collected ECG signals were divided into epochs of 2s length. The VT or VFL ECG epochs correspond to shockable arrhythmia whereas ventricular ectopic beats, ventricular bigeminy, ventricular escape rhythm and sinus rhythm belong to non-shockable arrhythmia. A total of 54096 ECG epochs were considered out of which 48095 belong to non-shockable arrhythmia and the rest 6001 belong to shockable arrhythmia.

3. Methodology

The methodology used in this work is illustrated in Fig. 3. In our work, we utilized the ECG signal of two classes i.e. non-shockable and shockable rhythm. First, we filtered out noise from the raw data for the analysis. We performed a three band, three level decomposition and obtained seven sub-bands. To fulfill our purpose, we used dual channel wavelet filter banks. We then extracted features from the sub-bands and performed classification. We obtained the best results by using the combination of fuzzy entropy (FE), Renyi entropy (RE) and sample entropy (SE) features.

3.1. Analysis of ECG signals and wavelet decomposition

ECG signals change with time and are non-stationary in nature. For proper analysis of ECG signals, an optimal method with better simultaneous localization in time and frequency domains is required. Wavelets have inherently good localization in time as well as frequency domains simultaneously [1,32]. Therefore use of wavelets for proper analysis of ECG signals is a good approach. However, it is not possible to have exact localization in time as well as frequency domain due to restrictions imposed by uncertainty principle. The most commonly used wavelets are Daubechies's orthogonal-wavelets. But, they do not

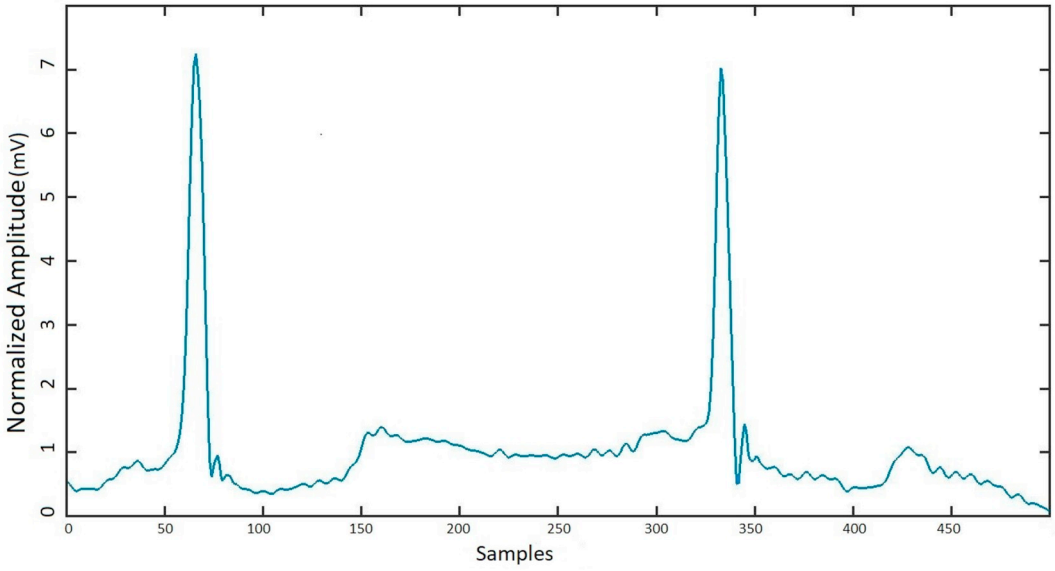

Fig. 1. Nonshockable rhythm.

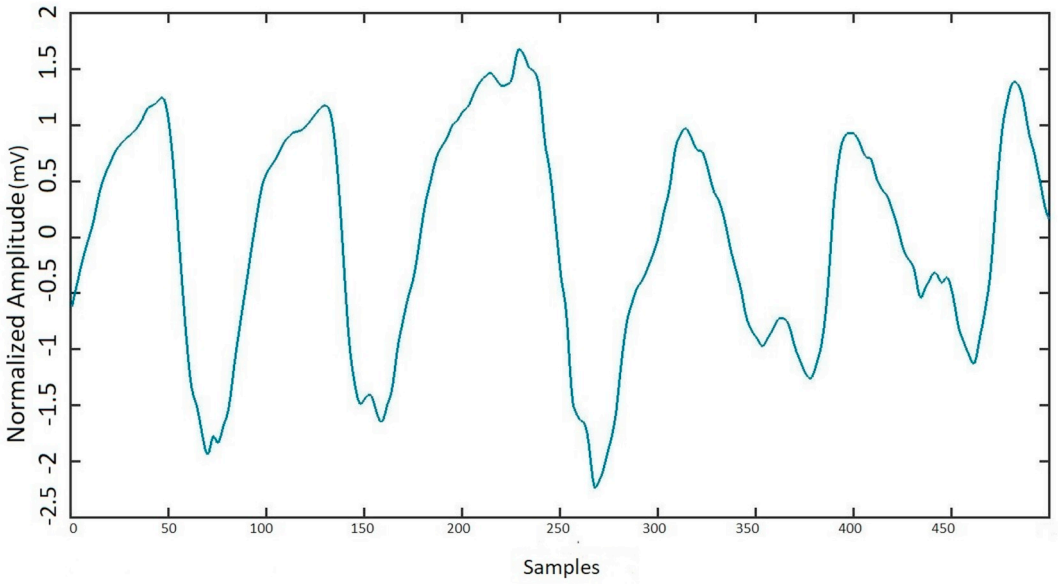

Fig. 2. Shockable rhythm.

Table 1
Definitions of acronyms.

Abbreviations	Definition
ECG	Electrocardiogram
VT	Ventricular-Tachycardia
VF	Ventricular Fibrillation
SBs	Sub-Bands
FE	Fuzzy Entropy
SE	Sample Entropy
RE	Renyi Entropy
SVM	Support Vector Machine
REM	Rapid Eye Movement
NSAR	Nonshockable Rhythm
SAR	Shockable Rhythm
OWFB	Orthogonal Wavelet Filter Bank
CHF	Congestive Heart Failure
HRV	Heart Rate Variability
ECG	Electrocardiogram
CAD	Coronary Artery Disease
mV	Millivolts
Accr	Accuracy
Sens	Sensitivity
Specs	Specificity
ROC	Receivers operating characteristic

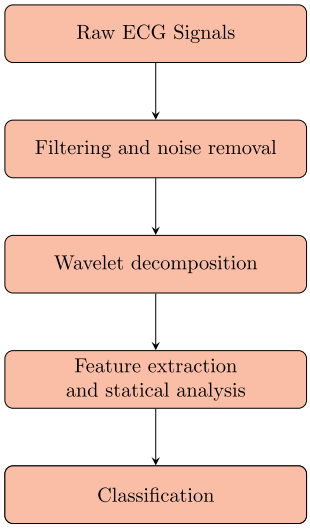

Fig. 3. Proposed methodology.

provide optimal time-frequency localization. Recent researches in the field of wavelet filter designing have shown that it is possible to design such a filter bank which gives optimal time-frequency localization. We used dual channel wavelet filter banks designed by Sharma et al. [33] for wavelet decomposition of ECG signals.

Wavelets are generated by using two band or three band filter banks (FBs). Dual band filter-banks have been [34] conventionally used for wavelet decomposition but they have limitations. The resolution of low frequency as well as high frequency bands are not satisfactory for level one decomposition. When such filter banks are cascaded, only the resolution of lower frequency range improves. Also, the two band filter has lower discrimination capability among the features extracted particularly when the signal has a high amount of energy in higher frequency bands. Furthermore, using multi level decomposition increases computation cost and linear phase can not be obtained [35]. Three band filter banks, on the other hand, have higher discrimination abilities, provided better resolution in lower frequency as well as higher frequency range, involving less computational cost and performed satisfactorily in digital watermarking, removing noise from images. Hence selection of three band orthogonal FBs for wavelet decomposition is the more efficient and reliable choice [35].

3.2. Extracted features

Fuzzy Entropy(FE) is a measure of degree to which given pattern belongs to one particular class [33]. It provides the extent to which our data is similar to one or more classes. Mathematically, fuzzy entropy is the negative log of conditional probability of a pattern being similar to two different classes.

Renyi Entropy feature (RE) Renyi Entropy is given as negative the natural logarithm of energy present in a signal sequence [36]. Mathematically, it is written as:

$$RenE_i = -Log\sum_{n\in Z}\left|g(n)\right|^2$$

where $g(n)$ is the signal sequence.

Sample Entropy(SE) Sample entropy is a feature that gives us a

measure of the degree of complexity in a system [37]. Mathematically, sample entropy is the negation of natural logarithm of conditional probability that epochs of length L matching point to point with some tolerance of x will also match at the upcoming point.

3.3. Classifiers

In this work, we have used k-nearest neighbors algorithm (KNN), SVM, linear discriminant analysis, logistic regression, RUSBoosted trees and complex trees to find the best performing one [38].

4. Three-band orthogonal wavelet filter banks

A 3-band filter bank is shown in Fig. 4. It is a combination of analysis and synthesis filter banks. Analysis filter-banks consist of three filters namely low-pass filter (ALPF) $G_0(z)$ on analysis side, band-pass filter (ABPF) $G_1(z)$ on analysis side and high-pass filter (AHPF) $G_2(z)$ on analysis side. Synthesis filter banks also consist of three filters namely, lowpass filter (SLPF) $S_0(z)$ on synthesis side, band-pass filter (SBPF) $S_1(z)$ on the synthesis side and high-pass filter (SHPF) $S_2(z)$ on the synthesis side.

A major difference between a 2-band and a 3-band filter is that the signal passing through the analysis filter bank in 2-band filter gets down-sampled with a factor of 2 after each iteration whereas it gets down-sampled with a factor 3 in case of 3-band filter [35]. Further, the signal while passing through filter banks on the synthesis side goes through up-sampling by a factor of 2 for 2-band filter bank whereas in case of 3-band filter bank, it gets up-sampled by a factor of 3.

Also, in case of 2-band filter banks, one scaling function and one wavelet function is generated, on the other hand, one scaling function and two wavelet functions are generated for 3-band filter bank. With the 3-band filter banks, a significant improvement is seen in resolution of higher frequencies. Also, the wavelets obtained from 3-band filter banks have improved time-frequency localization. An added advantage of 3-band filter banks is that we have orthogonality and linear phase simultaneously which is not possible with 2-band filter banks [35].

4.1. Designing of three band time-bandwidth minimized filter banks

The filter bank design problem is converted into a optimization problem. The optimal filter is obtained as the global solution for the proposed optimization problem. In the optimization process, the objective is to minimize the newly proposed time-frequency product of iterated filter banks. The constrains are orthogonality and regularity [39].

To design three band time-bandwidth minimized filter banks with time as well as frequency localization, our aim is to minimize the time-frequency product.

Let sequence be $s(n)$, time-variance t_v and time-mean x_0 [40]:

$$x_0 = \sum n|s(n)|^2 \tag{1}$$

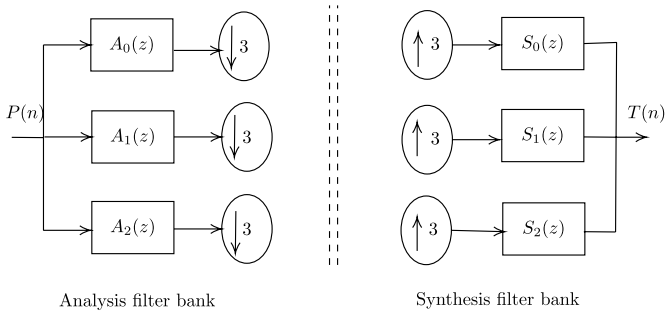

Fig. 4. Two-channel OWFB.

$$t_v^2 = \sum (n-n_0)^2|s(n)|^2 \tag{2}$$

For $s(n)$ to be a low-pass sequence, frequency-mean ω_o and frequency-variance t_ω is expressed as [40]:

$$\omega_o = 0 \tag{3}$$

$$t_v^2 = \frac{1}{2\pi}\int_{-\pi}^{\pi}(\omega-\omega_o)^2|S(\omega)|^2 d\omega \tag{4}$$

Time-frequency product of sequence $s(n)$ is given by x_1 which is given by the product of time-variance and frequency-variance of $s(n)$. The inequality condition of time-frequency product of low pass sequence is:

$$x_1 = t_v^2\omega_o^2 \geq \frac{(1-|S(\pi)|)^2}{4} \tag{5}$$

For $s(n)$ to be a band-pass sequence, frequency-mean ω_o and frequency-variance t_ω is expressed as:

$$\omega_o = \frac{1}{\pi}\int_0^{\pi}(\omega)^2|S(\omega)|^2 d\omega \tag{6}$$

$$t_\omega^2 = \frac{1}{\pi}\int_0^{\pi}(\omega-\omega_o)^2|S(\omega)|^2 d\omega \tag{7}$$

The lower bound of time-frequency product of band pass sequence is:

$$x_1 = t_\omega^2 t_v^2 \geq \frac{(1-\mu)^2}{4} \tag{8}$$

$$\mu = \frac{\omega_o}{\pi}\left|S(0)\right|^2 + \left(1-\frac{\omega_o}{\pi}\right)\left|S(\pi)\right|^2 \tag{9}$$

For $s(n)$ to be a high-pass sequence, frequency-mean ω_o and frequency-variance t_ω is expressed as:

$$\omega_o = \pi \tag{10}$$

$$t_\omega^2 = \frac{1}{2\pi}\int_{-\pi}^{\pi}(\omega-\omega_o)^2|S(\omega)|^2 d\omega \tag{11}$$

The lower bound of time-frequency product of high pass sequence is:

$$x_1 = t_\omega^2 t_v^2 \geq \frac{(1-|S(0)|)^2}{4} \tag{12}$$

Other equality conditions regarding S(ω) are:

$$1)\ For\ lowpass, S(\omega)=0 \quad at\ \ \omega=\pi \tag{13}$$

$$2)\ For\ bandpass, S(\omega)=0 \quad at\ \ \omega=0,\pi \tag{14}$$

$$3)\ For\ Highpass, S(\omega)=0 \quad at\ \ \omega=0 \tag{15}$$

If above condition are satisfied then following holds;

$$x_1 = t_\omega^2 t_v^2 \geq \frac{1}{4} \tag{16}$$

Hence, we get a new method of time-frequency localization which holds true for any given random sequence. First trigonometric moment Λ can be defined in the form [40]:

$$\Lambda = \frac{1}{2\pi}\int_{-\pi}^{\pi} e^{j\omega}|S(\omega)|^2 d\omega \tag{17}$$

$$\Lambda = \sum_{-\infty}^{\infty} s_n s_{n+1}^* \tag{18}$$

where n belongs to set of integers.

The frequency mean ω_o can be given by Ref. [40]:

$$\omega_o = 1-\Lambda \tag{19}$$

The frequency variance t_ω is given by Ref. [40]:

$$t_\omega = \frac{1-|\Lambda|^2}{|\Lambda|^2} = \left|\frac{1}{\sum_{-\infty}^{\infty} s_n s_{n+1}^*}\right|^2 - 1 \tag{20}$$

Λ is meaningful only when $\Lambda \neq 0$. The time-frequency product in its new form can be represented as [40]:

$$x_1 = t_\omega^2 t_v^2 \geq 0.25 \tag{21}$$

4.2. Parallel filter banks

To decompose a signal in $2M+1$ sub-bands M stages iterations are performed using three-band filter [39]. Hence to have seven sub-bands, three iterations are required using three-band filter. In Fig. 5 shown below, the topmost filter represents a low pass filter, the middle-one represent a band-pass filter and the bottom most filter represents a high-pass filter.

Let A_2 be a high pass filter and A_l be a filter which is band-pass and A_0 be a low-pass filter. The equations for parallel configuration of filters are given as [39]:

$$A_0^m(z) = \prod_0^{m-1} A_0\left(z^3\right)^k \tag{22}$$

$$A_1^i\left(z\right) = \left(A_1\left(z^{3(i-1))}\prod_0^{i-2} A_0\left(z^3\right)^k \quad i=2,3,\ldots,m\right) \tag{23}$$

$$A_2^i\left(z\right) = A_2\left(z^{3(i-1)}\prod_0^{i-2} A_0\left(z^3\right)^k \quad i=2,3,\ldots,m \tag{24}$$

The main aim is to reduce the time-frequency product of the components of filter banks namely high pass, low pass and band pass filters after every iteration.

4.3. Objective function and optimization

For designing of orthogonal filter banks with time as well as frequency localization, our aim is to minimize the weighted summation of all the time-frequency products of the parallel filter banks subject to orthogonality and constraints of regularity. For M = 3 we need to minimize the below function [35]:

$$\phi = x_1 y_1 + x_2 y_2 + \ldots . x_7 y_7 \tag{25}$$

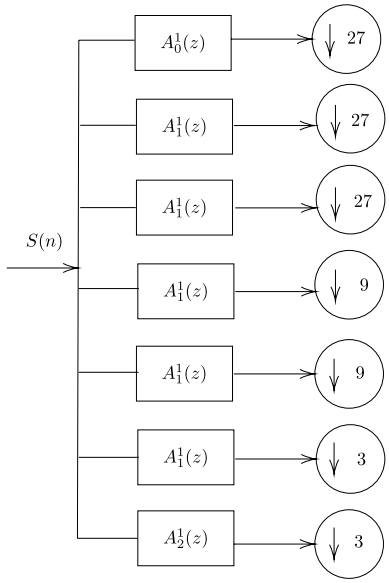

Fig. 5. Parallel filter banks.

where x_i are the time-frequency product and y_i are the weights assigned and sum of all weights is 1. The above equation is our objective function. The filter bank designing problem is now formulated as an optimization problem with constraints with the help of parametrization techniques given below [39]:

$$min_\theta(\phi) \tag{26}$$

subject to:

$$< A_l[n], A_m[n-y] > \delta(l-n)\delta(y) \quad l,n = 0,1,2 \tag{27}$$

alongwith

$$A_0\left(e^{j2\pi/3}\right) = A_0\left(e^{j4\pi/3}\right) = 0 \tag{28}$$

The above represents regularity constraint and triple-shift orthogonality. The set containing free parameters is θ_i. By reducing the value of ϕ three filters are obtained A_0 ,A_1,A_2. In above equations, δ represents impulse response.

However the con of this method is the number of free-variables is directly proportional to length of filter. So, for higher order filter the calculation increases. So a paraunitary structure is utilized in which polyphase matrix F(z) is simplified to N-paraunitary blocks P(z) by decomposition [40].

$$F(z) = P_N(z)P_{N-1}(z)\ldots .P_1F_0 \tag{29}$$

P_m(z) can be again factorised as:

$$P_m(z) = I - P_m(z)P_m^T + z^- P_m(z)P_m \tag{30}$$

Here P_m is column vector with same length as the number of bands of filter (3 for our case). After satisfying the orthogonality and regularity criteria the number of required free variables to design the filter is decreased. The optimization problem becomes un-constrained if the number of free variables becomes less than that required, using the following technique of parametrization as proposed by other researchers [41].

$$v_m(\theta_1,\theta_2) = [cos(\theta_1)cos(\theta_2) \quad cos(\theta_1)sin(\theta_2) \quad sin(\theta_1)]^T \tag{31}$$

The unconstrained optimization problem can be expressed as:

$$\left(A_0^i(n), A_1^i(n), A_2^i(n)\right) = argmin(\phi(\theta_i)) \tag{32}$$

where $A_0^i(n)$,$A_1^i(n)$,$A_2^i(n)$ form the coefficients of the bank. Finally the reconstruction condition can be used to find the coefficients of the filter bank. The steps involved to optimize the filter bank are given below [41]:

1) Select the filter length and the stages of decomposition.
2) Use paraunitary equations (19) and (20), technique for parametrization (21)
3) Unconstrained optimization problem is formulated (22).
4) By employing use of MATLAB optimization tool box objective function (15) is optimized.
5) Values of the optimization function are noted.

The process does not yield the optimal filter bank so the entire process is repeated until the required filter bank is obtained. The salient features of this filter bank are as follows:

1) In this paper three band filter band is used while others have used biorthogonal two wavelet channel filter banks.
2) In this paper time-frequency localization is unconstrained and can be used for arbitrary sequence unlike constrained time-frequency localization used by others.

3) Various researchers employed factorization of Lagrange half-based polynomial to obtain parametric expressions. We used paraunitary structure with Peng's method.
4) This paper refers to designing of wavelet bases with single regularity constraint while other researchers refer to wavelet bases with multiple regularity constraints [41].

5. Results

5.1. Feature extraction results

We have decomposed the signal into seven sub-bands. The p-values of all the extracted features for each sub-band is mentioned in Table 2. The statistical values (mean and standard deviation) of FE, RE and SE features obtained from all seven sub-bands along with their ranking are mentioned in Table 3, Table 4 and Table 5, respectively.

5.2. Classification results

We have then classified by using various combinations of features (individually and combining them). The confusion matrix in terms of true positive (TP), false positive (FP), true negative (TN), and false negative (FN) along with accuracy corresponding to the best classifier are presented. The receiver operating characteristics (ROC) curves showing values of area under curve (AUC) are also provided.

5.2.1. Classification of data obtained using FE feature

Using this feature, we obtained a maximum accuracy of 96.4% with medium Gaussian support vector machine (SVM). The AUC for the obtained ROC curve (Fig. 6) obtained is 0.93. We trained different models and the classification results are shown in Table 6.

The confusion matrix obtained using the FE feature corresponding to the model that gave the best accuracy (Gaussian SVM) is given in Table 7. Fig. 6 exhibits the ROC curve obtained using FE feature alone with coarse KNN classifier.

5.2.2. Classification of data obtained using RE feature

Using this feature, we obtained a maximum accuracy of 93.4% with fine Gaussian SVM. The AUC obtained for the ROC curve (Fig. 7) is 0.91. We trained different models based on this data and the accuracy results corresponding to different models are obtained as shown in Table 8.

The confusion matrix for classification of data obtained through FE feature corresponding to the model that gave best accuracy (fine Gaussian SVM) is shown in Table 9.

5.2.3. Classification of data obtained through SE feature

Using this feature, we obtained maximum accuracy of 88.9% using coarse KNN. We trained different models using this data and the classification results are shown in Table 10. Classifications are done on a 10-fold cross validation scheme.

The confusion matrix for classification of data obtained through SE feature corresponding to the model that gave best accuracy (coarse KNN) is shown in Table 11 and the ROC curve is shown in Fig. 8.

Table 2
The p-values of features extracted from signals.

Sub-bands	FE	RE	SE
SB-1	7.567×10^{-153}	0	2.652×10^{-22}
SB-2	0	0	0.584
SB-3	0	0	0.101
SB-4	0	0	0.584
SB-5	0	0	0.101
SB-6	1.237×10^{-76}	2.174×10^{-31}	0.584
SB-7	2.322×10^{-171}	4.173×10^{-255}	0.101

Table 3
Ranking of FE sub-bands and their statistical values (*mean* ± *standard deviation*).

SBs	FE		
	Non-shockable	Shockable	Rank
SB-1	0.291 ± 0.142	-4.215 ± 0.215	1
SB-2	0.258 ± 0.136	-3.542 ± 0.201	3
SB-3	0.089 ± 0.056	-2.354 ± 1.555	8
SB-4	0.081 ± 0.052	-7.140 ± 0.828	10
SB-5	1.463 ± 0.904	-3.561 ± 0.073	11
SB-6	1.019 ± 0.502	-5.525 ± 1.691	12
SB-7	1.029 ± 0.514	-5.460 ± 0.864	13

Table 4
Ranking of RE sub-bands and their statistical values (*mean* ± *standard deviation*).

SBs	RE		
	Non-shockable	Shockable	Rank
SB-1	-6.232 ± 1.308	-4.211 ± 1.011	2
SB-2	-5.610 ± 1.191	-3.542 ± 1.149	4
SB-3	-4.119 ± 1.303	-2.354 ± 1.234	5
SB-4	-6.522 ± 0.771	-7.141 ± 0.467	6
SB-5	-5.201 ± 1.211	-3.561 ± 1.555	7
SB-6	-5.989 ± 1.084	-5.526 ± 0.828	9
SB-7	-5.601 ± 0.783	-5.461 ± 0.747	14

Table 5
Ranking of SE sub-bands and their statistical values (*mean* ± *standard–deviation*).

SBs	SE		
	Non-shockable	Shockable	Rank
SB-1	0.634 ± 0.222	0.658 ± 0.238	15
SB-2	0.653 ± 0.422	0.652 ± 0.417	19
SB-3	0.613 ± 0.376	0.598 ± 0.368	17
SB-4	0.653 ± 0.422	0.652 ± 0.417	21
SB-5	0.613 ± 0.376	0.598 ± 0.368	16
SB-6	0.653 ± 0.422	0.652 ± 0.418	20
SB-7	0.613 ± 0.376	0.598 ± 0.368	18

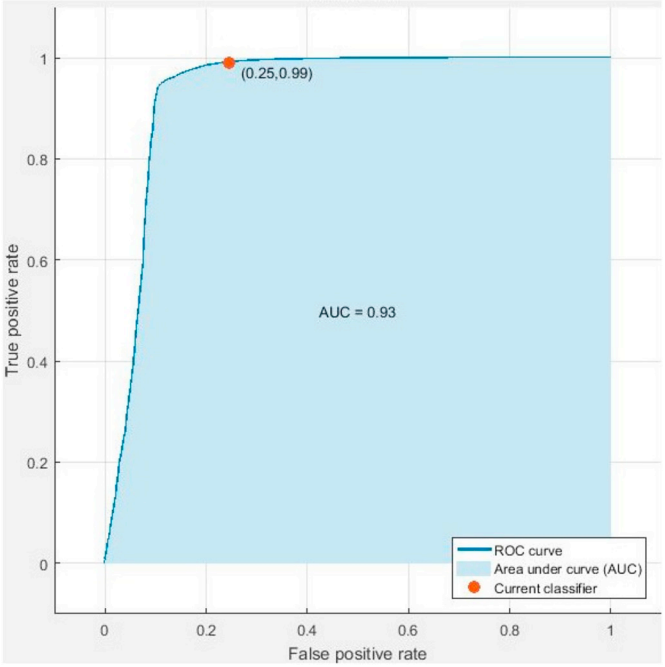

Fig. 6. ROC curve obtained using FE feature alone with coarse KNN classifier.

Table 6
Summary of accuracy (%) obtained for different classifiers.

Classifier	Accuracy (%)
Linear discriminant	90.8
RUSBoosted Trees	94.4
KNN	94.6
Logistic Regression	96.2
Complex Trees	96.2
Gaussian SVM	**96.4**

Table 7
Confusion matrix for 2 class classification for FE.

True/predicted	0	1
0(NSAR)	47641	454
1(SAR)	1471	4530

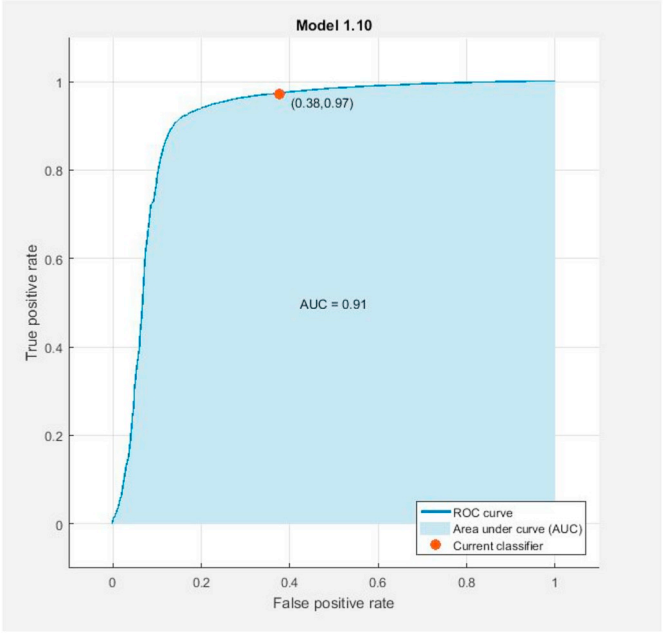

Fig. 7. ROC curve obtained using RE feature alone with coarse KNN classifier.

Table 8
Summary of the accuracy (%) obtained using different classifiers.

Classifier	Accuracy (%)
Linear discriminant	89.5
Logistic Regression	90.0
Complex Trees	91.9
Bagged trees	93.0
KNN	93.2
Gaussian SVM	**93.4**

Table 9
Confusion matrix for 2 class classification using RE alone.

True/predicted	0	1
0(NSAR)	46797	1298
1(SAR)	2262	3739

5.2.4. Classification of data obtained through combining the features (FE, RE and SE)

After classifying the data individually, we performed classification by combining the three features to confirm the possible improvement in the accuracy. We found that the maximum accuracy increased to 98.9% using cubic SVM model.

Different accuracies are obtained corresponding to different classification models as shown in Table 12. Classifications are done using a 10-fold cross validation scheme.

The confusion matrix for classification of data obtained through FE feature with fine Gaussian SVM gave best accuracy and is shown in Table 13, and the corresponding ROC curve is shown in Fig. 9. Table 14 gives better comprehension of all the classification results.

Table 10
Summary of the accuracy (%) obtained using different classifiers.

Classifier	Accuracy (%)
Cubic SVM	77.1
Bagged trees	80.1
Complex Trees	88.6
Linear discriminant	88.9
KNN	**88.9**

Table 11
Confusion matrix for 2 class classification using SE alone.

True/predicted	0	1
0(NSAR)	48064	31
1(SAR)	5980	21

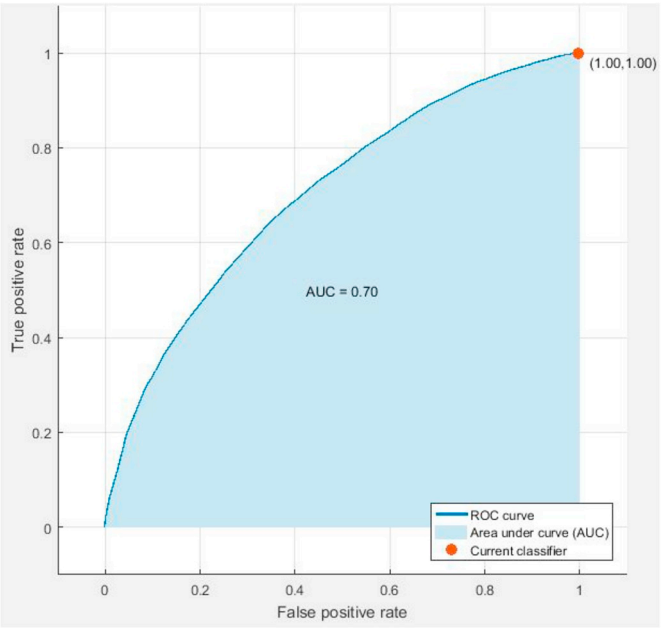

Fig. 8. ROC curve obtained using SE feature alone with SVM classifier.

Table 12
Summary of accuracy (%) obtained for different classifiers.

Classifier	Accuracy (%)
Linear discriminant	90
Logistic Regresssion	97.3
Complex Trees	98
Bagged trees	98.6
Cubic SVM	**98.9**

Table 13
Confusion matrix for 2 class classification obtained using combined features.

True/predicted	0	1
0(NSAR)	47930	165
1(SAR)	445	556

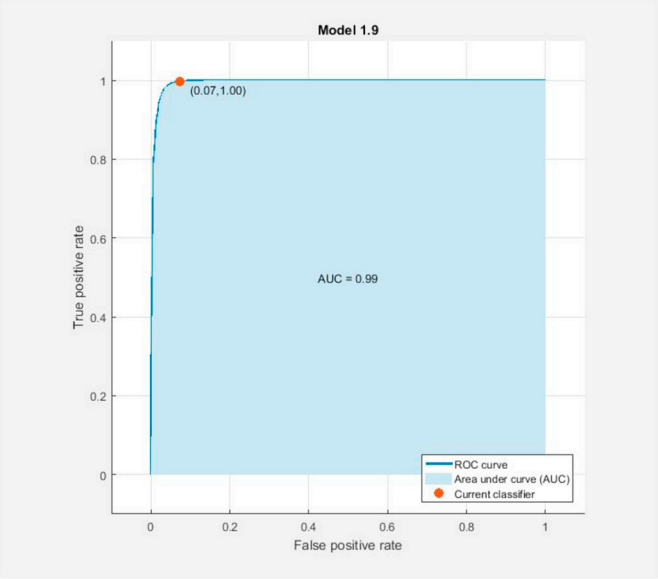

Fig. 9. ROC curve obtained using combined features with SVM classifier.

Table 14
Overall classification results obtained with SVM classifier.

Features	TP	TN	FP	FN	Acc (%)	Sens (%)	Specs (%)
RE	46797	3739	1298	2262	93.41	95.38	74.23
FE	47641	4530	454	1471	96.44	97.00	90.89
SE	48064	21	31	5980	88.88	88.93	40.38
FE + RE	47639	4923	456	1078	97.16	99.05	82.03
SE + RE	47942	5265	153	736	98.35	**99.68**	87.73
SE + FE	47774	5107	321	894	97.75	99.33	85.10
FE + RE + SE	47930	5556	165	445	**98.87**	99.08	**97.11**

6. Discussion

The wavelet based methods have been used previously for classification of physiological signals using Daubechies two-band wavelet filter banks [42]. The features extracted from these filter banks may not be optimal for time-frequency localization [43,44]. In the proposed method, a whole new class of wavelet based filter banks have been employed. We used 3-band wavelet filter banks [40] for wavelet decomposition of ECG signals as the wavelets from these filter banks are optimal. Methods involving 3-band wavelet-based signal features have hitherto not been explored by researchers for detecting shockable arrhythmia. The novelty of our work is that we used optimal 3-band wavelet based features for the classification of shockable and non-shock able arrhythmia, and the proposed method has surpassed all existing models in terms of classification performance. Hence, the proposed method yields the most accurate model available till day.

Also, for detecting shockable arrhythmia, epochs of duration 8s or 10s have normally been used whereas we have employed epochs of only 2s duration, which yielded high accuracy for classification of shockable and non-shockable rhythm [33].

The mean value of FE is higher for non-shockable than shockable one in all the sub-bands. The mean value of RE feature is higher for shockable than non-shockable one in all the sub-bands except SB-4. In case of the SE feature mean value is almost same for non-shockable and shockable one in all the sub-bands.

From above, the features (wavelet-based) of FE performed much better than the other two features (RE and SE) in terms of sensitivity, accuracy and specificity. FE alone gave the best classification results in disseminating the two classes. After combining the three features, we obtained significantly improved classification results. In various automated systems, different window lengths (WL) (10s,8s,6s, 5s and 2s)are used for processing ECG epochs [44–46]. A short window length is always desirable for fast implementation. In this work, we used the shortest window length (2s). It is worthwhile to note that though we used epoch of shortest duration, our classification results are better than previous works. Another advantage of this methodology is that the pre-processing of raw data is not complex like other reported works [44–46]. Except for sample entropy, the p-values of the remaining features are almost close to zero and hence they are quite significant for classification. From Table 11, it is evident that SB-1 corresponding to the FE feature is ranked first and SB-4 corresponding to SE feature is ranked the last. These rankings have been done based on t-tests. All experiments and classifications are performed using MATLAB software with Intel's Xeon processor clocked at 3.5 GHz and with 16 GB of RAM. The model took approximately 81.82 s for classification at a predicted speed of approximately 67000 obs/secs. We employed optimal wavelet-based feature extraction using 3-band wavelet filter banks and obtained much better classification results than Tripathy et al. [47,48]. Also, the computational cost of our method is lesser than variational mode decomposition (VMD).

Sometimes, accuracy may be misleading and hence they are not used for performance analysis. Other parameters like area under curve (AUC) and F1 score are also used to judge the classification results. In our method, we have obtained AUC to be equal to 0.99 which is very close to

Table 15
Comparison of automated shockable and non-shockable system using ECG signals.

Reference (Year)	Methodology/WL	Performance
[49]	Five previously proposed methods reviewed-10s	Sens: 94%
(2000)		Specs: 91%
[50]	Band-pass Filtering-10s	Sens: 94.45%
(2004)		Specs: 95.9%
[51]	Time delay method-	Sens: 79%
(2007)	(twelve different)-8s	Specs: 98.5%
		Accr: 96.2%
[52] (2007)	discriminant analysis-10s	Sens: 94.1%
		Specs: 93.8%
[18]	distribution analysis	Sens: 97%
(2007)	based on amplitude-6s	Specs: 98%
		Accr: 98%
[10] (2014)	Morphological, complexity and spectral feature of heart signals	Sen: 92%
	support vector machine-8s	Specs: 97%
[53](2014)	VF-filter leakage measures	Sens: 96.2%
	auxiliary count	Specs: 96.2%
	Support Vector Machine-5s	Accr: 96.3%
[54]	Variational mode decomposition (VMD)	Sens: 96.54%
(2016)	Permutation Entropy and Renyi Entropy	Specs:97.97%
	Classifier-random forest-8s	Accr: 97.23%
[9]	Convolution of Neural	Sens: 95.32%
(2018)	Network (CNN)-2s	Specs:91.04%
		Accr: 93.18%
In the current work	**Extracted features:**	
	• FE-2s	**Sens: 99.66%**
	• RE-2s	**Spes: 98.35%**
	• SE-2s	**Accr:98.87%**
	Classification Method:	
	• SVM	F1-score:0.994

the ideal value which is 1. Also, our F1-score is 0.9937 (from Table 15), is close to the ideal value of 1. Hence our proposed system has performed well in discriminating the two arrhythmias. The VT and VF with heart rate more than 180 beats/min can be dangerous and can lead to life threatening brain injury and ultimately may lead to death in case the patient is not treated with defibrillation shocks within a critical time. In both cases (VF and VT), heart rate is high; hence, a fast as well as appropriate algorithm which automatically detects is needed for an automated external defibrillator (AED) system.

7. Conclusion

In our proposed methodology automated discrimination of non-shockable and shockable arrhythmia using ECG signals is analyzed using features extracted from optimal wavelets. In this work, we used optimal three channel wavelet filter banks to obtain the sub-bands of the ECG epochs. The proposed system showed significant capability in the detection of shockable arrhythmia by employing the proposed filter banks. The FE, RE, and SE features extracted from the sub-bands of ECG samples are fed to different classifiers. We have obtained an overall accuracy of 98.9% using the SVM classifier. Hence the proposed methodology employing three channel wavelet based entropy features is suitable for diagnosis of shockable arrhythmia and implementation in automated defibrillators.

Further, we have used ECG epochs of shortest duration (2sec) thereby reducing the computational load significantly and hence making the system much faster and efficient. Another advantage of using optimal filter-bank centered features is that these features may be used in the diagnosis of other heart related disorders also. In this work, we have used only three entropy features. In future, more such non-linear features like Hurt exponent, fractal dimension, Lyponev exponents etc. can be used to improve the classification performance. Also, it would be interesting to employ deep learning based techniques such as convolutional neural network (CNN) in distinguishing shockable and non-shockable arrhythmia using a bigger database and employing the proposed wavelet filter as one of the layers of the CNN. Cloud based systems can be developed where this model can be placed and can be used to test the patients in ICU etc. Also, we may use feature learning-based approaches. In future, we intend to use other deep learning techniques for study such as long short term memory (LSTM) and autoencoders. We can also implement various data balancing techniques to handle the data imbalance problem.

References

[1] C. Flavell, L.W. Stevenson, Take heart with heart failure, Circulation 104 (18) (2001) e89–e91, https://doi.org/10.1161/hc4301.099136.

[2] C. Yancy, M. Jessup, B. Bozkurt, J. Butler, D. Casey, M. Drazner, G. Fonarow, S. Geraci, T. Horwich, J. Januzzi, M. Johnson, E. Kasper, W. Levy, F. Masoudi, P. McBride, J. McMurray, J. Mitchell, P. Peterson, B. Riegel, F. Sam, L. Stevenson, W. Tang, E. Tsai, B. Wilkoff, accf/aha guideline for the management of heart failure: executive summary: a report of the american college of cardiology foundation/american heart association task force on practice guidelines, Circulation 128 (16) (2013) 1810–1852, https://doi.org/10.1161/CIR.0b013e31829e8807, 2013.

[3] M. Sharma, U.R. Acharya, A new method to identify coronary artery disease with ecg signals and time-frequency concentrated antisymmetric biorthogonal wavelet filter bank, Pattern Recognit. Lett. 125 (2019) 235–240. https://doi.org/10.1016/j.patrec.2019.04.014. http://www.sciencedirect.com/science/article/pii/S0167865519301217.

[4] Q. Li, C. Rajagopalan, G.D. Clifford, Ventricular fibrillation and tachycardia classification using a machine learning approach, IEEE (Inst. Electr. Electron. Eng.) Trans. Biomed. Eng. 61 (6) (2014) 1607–1613, https://doi.org/10.1109/TBME.2013.2275000.

[5] A.S. Khaled, M.I. Owis, A.S. Mohamed, Employing time-domain methods and poincaré plot of heart rate variability signals to detect congestive heart failure, BIME journal 6 (1) (2006) 35–41 (n/a).

[6] N.D. Gillespie, The diagnosis and management of chronic heart failure in the older patient, Br. Med. Bull. 75–76 (1) (2006) 49–62, https://doi.org/10.1093/bmb/ldh060. http://oup.prod.sis.lan/bmb/article-pdf/75-76/1/49/25152183/ldh060.pdf. https://dx.doi.org/10.1093/bmb/ldh060.

[7] M. Hadase, A. Azuma, K. Zen, S. Asada, T. Kawasaki, T. Kamitani, S. Kawasaki, H. Sugihara, H. Matsubara, Very low frequency power of heart rate variability is a powerful predictor of clinical prognosis in patients with congestive heart failure, Circ. J. 68 (4) (2004) 343–347, https://doi.org/10.1253/circj.68.343. https://doi.org/10.1253/circj.68.343.

[8] A. Bhurane, M. Sharma, R. San-Tan, U.R. Acharya, An efficient detection of congestive heart failure using frequency localized filter banks for the diagnosis with ecg signals, Cognitive Systems Research 55 (2019) 82–94, https://doi.org/10.1016/j.cogsys.2018.12.017. http://www.sciencedirect.com/science/article/pii/S1389041718308568.

[9] U.R. Acharya, H. Fujita, S.L. Oh, U. Raghavendra, J.H. Tan, M. Adam, A. Gertych, Y. Hagiwara, Automated identification of shockable and non-shockable life-threatening ventricular arrhythmias using convolutional neural network, Future Gener. Comput. Syst. (2018), https://doi.org/10.1016/j.future.2017.08.039.

[10] F. Alonso-Atienza, E. Morgado, L. Fernandez-Martinez, A. Garcia-Alberola, J. L. Rojo-Álvarez, Detection of life-threatening arrhythmias using feature selection and support vector machines, IEEE Trans. Biomed. Eng. 61 (2014), https://doi.org/10.1109/TBME.2013.2290800.

[11] U. Rajendra Acharya, K. Paul Joseph, N. Kannathal, C.M. Lim, J.S. Suri, Heart rate variability: a review, Med. Biol. Eng. Comput. 44 (12) (2006) 1031–1051, https://doi.org/10.1007/s11517-006-0119-0. https://doi.org/10.1007/s11517-006-0119-0.

[12] U.R. Acharya, M. Sankaranarayanan, J. Nayak, C. Xiang, T. Tamura, Automatic identification of cardiac health using modeling techniques: a comparative study, Inf. Sci. 178 (23) (2008) 4571–4582, including Special Section: Genetic and Evolutionary Computing, https://doi.org/10.1016/j.ins.2008.08.006, http://www.sciencedirect.com/science/article/pii/S0020025508003381.

[13] M. Sharma, S. Agarwal, U.R. Acharya, Application of an optimal class of antisymmetric wavelet filter banks for obstructive sleep apnea diagnosis using ecg signals, Comput. Biol. Med. 100 (2018) 100–113. https://doi.org/10.1016/j.compbiomed.2018.06.011. http://www.sciencedirect.com/science/article/pii/S0010482518301598.

[14] M. Sharma, D. Goyal, P. Achuth, U.R. Acharya, An accurate sleep stages classification system using a new class of optimally time-frequency localized three-band wavelet filter bank, Comput. Biol. Med. 98 (2018) 58–75. https://doi.org/10.1016/j.compbiomed.2018.04.025. http://www.sciencedirect.com/science/article/pii/S0010482518301069.

[15] S. Shah, M. Sharma, D. Deb, R.B. Pachori, An automated alcoholism detection using orthogonal wavelet filter bank, in: 2017 International Conference on Machine Intelligence and Signal Processing (MISP), 2017.

[16] M. Sharma, R.S. Tan, U.R. Acharya, A novel automated diagnostic system for classification of myocardial infarction ecg signals using an optimal biorthogonal filter bank, Computers in Biology and Medicine 102 (2018) 341–356, https://doi.org/10.1016/j.compbiomed.2018.07.005. http://www.sciencedirect.com/science/article/pii/S0010482518301884.

[17] A. Amann, R. Tratnig, K. Unterkofler, Detecting ventricular fibrillation by time-delay methods, IEEE (Inst. Electr. Electron. Eng.) Trans. Biomed. Eng. 54 (1) (2007) 174–177, https://doi.org/10.1109/TBME.2006.880909.

[18] S. Fokkenrood, P. Leijdekkers, V. Gay, Ventricular tachycardia/fibrillation detection algorithm for 24/7 personal wireless heart monitoring, in: T. Okadome, T. Yamazaki, M. Makhtari (Eds.), Pervasive Computing for Quality of Life Enhancement, Springer Berlin Heidelberg, Berlin, Heidelberg, 2007, pp. 110–120.

[19] J. Li, B.E. Carlson, A.A. Lacis, Application of spectral analysis techniques in the inter-comparison of aerosol data, part 4: synthesized analysis of multisensor satellite and ground-based aod measurements using combined maximum covariance analysis, Atmos. Meas. Tech. 7 (2014) 2531–2549, https://doi.org/10.5194/amt-7-2531-2014.

[20] R.K. Tripathy, L.N. Sharma, S. Dandapat, Detection of shockable ventricular arrhythmia using variational mode decomposition, J. Med. Syst. 40 (4) (2016) 79, https://doi.org/10.1007/s10916-016-0441-5. https://doi.org/10.1007/s10916-016-0441-5.

[21] U.R. Acharya, S.L. Oh, Y. Hagiwara, J.H. Tan, H. Adeli, Deep convolutional neural network for the automated detection and diagnosis of seizure using eeg signals, Comput. Biol. Med. 100 (2018) 270–278. https://doi.org/10.1016/j.compbiomed.2017.09.017. http://www.sciencedirect.com/science/article/pii/S0010482517303153.

[22] J. Zala, M. Sharma, R. Bhalerao, Tunable q - wavelet transform based features for automated screening of knee-joint vibroarthrographic signals, in: 2018 International Conference on Signal Processing and Integrated Networks (SPIN), 2018.

[23] M. Sharma, P. Sharma, R.B. Pachori, V.M. Gadre, Double density dual-tree complex wavelet transform based features for automated screening of knee-joint vibroarthrographic signals, in: Machine Intelligence and Signal Analysis. Advances in Intelligent Systems and Computing, vol. 748, Springer, Singapore, 2019, pp. 279–290.

[24] M. SHARMA, S. SHAH, A novel approach for epilepsy detection using time–frequency localized bi-orthogonal wavelet filter, J. Mech. Med. Biol. (2019) 1940007.

[25] M. Sharma, U.R. Acharya, Analysis of knee-joint vibroarthographic signals using bandwidth-duration localized three-channel filter bank, Comput. Electr. Eng. 72 (2018) 191–202. https://doi.org/10.1016/j.compeleceng.2018.08.019. http://www.sciencedirect.com/science/article/pii/S0045790618311017.

[26] M. Sharma, P. Sharma, R.B. Pachori, U.R. Acharya, Dual-tree complex wavelet transform-based features for automated alcoholism identification, Int. J. Fuzzy Syst. 20 (5) (2018) 1297–1308. https://doi.org/10.1007/s40815-018-0455-x. https://link.springer.com/article/10.1007/s40815-018-0455-x.

[27] S.L. Oh, E.Y. Ng, R.S. Tan, U.R. Acharya, Automated beat-wise arrhythmia diagnosis using modified u-net on extended electrocardiographic recordings with heterogeneous arrhythmia types, Comput. Biol. Med. 105 (2019) 92–101.
[28] O. Faust, A. Shenfield, M. Kareem, T.R. San, H. Fujita, U.R. Acharya, Automated detection of atrial fibrillation using long short-term memory network with rr interval signals, Comput. Biol. Med. 102 (2018) 327–335. https://doi.org/10.1016/j.compbiomed.2018.07.001. http://www.sciencedirect.com/science/article/pii/S0010482518301847.
[29] S.L. Oh, E. Ng, R.S. Tan, U.R. Acharya, Automated diagnosis of arrhythmia using combination of cnn and lstm techniques with variable length heart beats, Comput. Biol. Med. 102 (2018), https://doi.org/10.1016/j.compbiomed.2018.06.002.
[30] M. Sharma, M. Raval, U.R. Acharya, A new approach to identify obstructive sleep apnea using an optimal orthogonal wavelet filter bank with ecg signals, Inform. Med. Unlocked (2019) 100170. https://doi.org/10.1016/j.imu.2019.100170. http://www.sciencedirect.com/science/article/pii/S235291481930022X.
[31] A.L. Goldberger, L.A. Amaral, L. Glass, J.M. Hausdorff, P.C. Ivanov, R.G. Mark, J. E. Mietus, G.B. Moody, C.-K. Peng, H.E. Stanley, Physiobank, physiotoolkit, and physionet, Circulation 101 (23) (2000) e215–e220.
[32] M. Sharma, R.-S. Tan, U.R. Acharya, Automated heartbeat classification and detection of arrhythmia using optimal orthogonal wavelet filters, Inform. Med. Unlocked (2019) 100221. https://doi.org/10.1016/j.imu.2019.100221. http://www.sciencedirect.com/science/article/pii/S2352914819301091.
[33] M. Sharma, A. Dhere, R.B. Pachori, U.R. Acharya, An automatic detection of focal EEG signals using new class of time–frequency localized orthogonal wavelet filter banks, Knowl. Based Syst. 118 (2017) 217–227.
[34] J. Wilbur, P. James, Diagnosis and management of heart failure in the outpatient setting, primary care: clinics in office practice, Cardiovasc. Dis. 32 (4) (2005) 1115–1129. https://doi.org/10.1016/j.pop.2005.09.005. http://www.sciencedirect.com/science/article/pii/S0095454305000801.
[35] M. Sharma, D. Goyal, A. PV, U.R. Acharya, An accurate sleep stages classification system using a new class of optimally time-frequency localized three-band wavelet filter bank, Comput. Biol. Med. 98 (2018), https://doi.org/10.1016/j.compbiomed.2018.04.025.
[36] M. Sharma, A.A. Bhurane, U.R. Acharya, MMSFL-OWFB, A novel class of orthogonal wavelet filters for epileptic seizure detection, Knowl. Based Syst. 160 (2018) 265–277. https://doi.org/10.1016/j.knosys.2018.07.019. http://www.sciencedirect.com/science/article/pii/S0950705118303721.
[37] U.R. Acharya, H. Fujita, V. K Sudarshan, S. Bhat, J.E.W. Koh, Application of entropies for automated diagnosis of epilepsy using eeg signals: a review, Knowl. Based Syst. 88 (2015), https://doi.org/10.1016/j.knosys.2015.08.004.
[38] R.O. Duda, P.E. Hart, D.G. Stork, Pattern Classification, John Wiley & Sons, 2012.
[39] M. Sharma, D. Deb, U.R. Acharya, A novel three-band orthogonal wavelet filter bank method for an automated identification of alcoholic EEG signals, Appl. Intell. (2017), https://doi.org/10.1007/s10489-017-1042-9.
[40] M. Sharma, D. Goyal, P. Achuth, U.R. Acharya, An accurate sleep stages classification system using a new class of optimally time-frequency localized three-band wavelet filter bank, Comput. Biol. Med. 98 (2018) 58–75. https://doi.org/10.1016/j.compbiomed.2018.04.025. http://www.sciencedirect.com/science/article/pii/S0010482518301069.
[41] M. Sharma, R.S. Tan, U.R. Acharya, Detection of shockable ventricular arrhythmia using optimal orthogonal wavelet filters, Neural Comput. Appl. (2019), https://doi.org/10.1007/s00521-019-04061-8.
[42] M. Sharma, A. Vanmali, V. Gadre, Wavelets and Fractals in Earth System Sciences, chap.Â Construction of Wavelets: Principles and Practices Â, 2013.
[43] D. Bhati, M. Sharma, R.B. Pachori, V.M. Gadre, Time-frequency localized three-band biorthogonal wavelet filter bank using semidefinite relaxation and nonlinear least squares with epileptic seizure EEG signal classification, Digit. Signal Process. 62 (2017) 259–273.
[44] M. Sharma, P.V. Achuth, R.B. Pachori, V.M. Gadre, A parametrization technique to design joint time–frequency optimized discrete-time biorthogonal wavelet bases, Signal Process. 135 (2017) 107–120.
[45] M. Sharma, R. B. Pachori, A novel approach to detect epileptic seizures using a combination of tunable-q wavelet transform and fractal dimension, Journal of Mechanics in Medicine and Biology 0 (0) (0) 1740003. arXiv:http://www.worldscientific.com/doi/pdf/10.1142/S0219519417400036, doi:10.1142/S0219519417400036. URL http://www.worldscientific.com/doi/abs/10.1142/S0219519417400036.
[46] M. Sharma, A. Dhere, R.B. Pachori, V.M. Gadre, Optimal duration-bandwidth localized antisymmetric biorthogonal wavelet filters, Signal Process. 134 (2017) 87–99.
[47] A. Narin, Y. Isler, M. Ozer, Investigating the performance improvement of HRV indices in CHF using feature selection methods based on backward elimination and statistical significance, Comput. Biol. Med. 45 (2014) 72–79, https://doi.org/10.1016/j.compbiomed.2013.11.016. https://doi.org/10.1016/j.compbiomed.2013.11.016.
[48] U. Orhan, Real-time CHF detection from ECG signals using a novel discretization method, Comput. Biol. Med. 43 (10) (2013) 1556–1562, https://doi.org/10.1016/j.compbiomed.2013.07.015. https://doi.org/10.1016/j.compbiomed.2013.07.015.
[49] I. Jekova, Comparison of five algorithms for the detection of ventricular fibrillation from the surface ecg, Physiol. Meas. 21 (2000) 429–439, https://doi.org/10.1088/0967-3334/21/4/301.
[50] I. Jekova, V. Krasteva, Real time detection of ventricular fibrillation and tachycardia, Physiol. Meas. 25 (2004) 1167–1178, https://doi.org/10.1088/0967-3334/25/5/007.
[51] A. Amann, R. Tratnig, K. Unterkofler, Detecting ventricular fibrillation by time-delay methods, IEEE (Inst. Electr. Electron. Eng.) Trans. Biomed. Eng. 54 (1) (2007) 174–177, https://doi.org/10.1109/TBME.2006.880909.
[52] I. Jekova, Shock advisory tool: detection of life-threatening cardiac arrhythmias and shock success prediction by means of a common parameter set, Biomed. Signal Process. Control 2 (2007) 25–33, https://doi.org/10.1016/j.bspc.2007.01.002.
[53] Q. Li, C. Rajagopalan, G.D. Clifford, Ventricular fibrillation and tachycardia classification using a machine learning approach, IEEE (Inst. Electr. Electron. Eng.) Trans. Biomed. Eng. 61 (6) (2014) 1607–1613, https://doi.org/10.1109/TBME.2013.2275000.
[54] R.K. Tripathy, L.N. Sharma, S. Dandapat, Detection of shockable ventricular arrhythmia using variational mode decomposition, J. Med. Syst. 40 (4) (2016) 79, https://doi.org/10.1007/s10916-016-0441-5. https://doi.org/10.1007/s10916-016-0441-5.